Linear optical pulse compression based on temporal zone plates

Bo Li,[1,2,*] Ming Li,[1,3] Shuqin Lou,[2] and José Azaña[1]

[1] *Institut National de la Recherche Scientifique – Energie, Matériaux et Télécommunications, Montréal, Québec, H5A 1K6 Canada*

[2] *School of Electronic and Information Engineering, Beijing Jiaotong University, Beijing, 10004, China*

[3] *Institute of Semiconductors, Chinese Academy of Sciences, No. 35, Tsinghua East Road, Beijing, 100083 China*

** bo.li@emt.inrs.ca*

Abstract: We propose and demonstrate time-domain equivalents of spatial zone plates, namely temporal zone plates, as alternatives to conventional time lenses. Both temporal intensity zone plates, based on intensity-only temporal modulation, and temporal phase zone plates, based on phase-only temporal modulation, are introduced and studied. Temporal zone plates do not exhibit the limiting tradeoff between temporal aperture and frequency bandwidth (temporal resolution) of conventional linear time lenses. As a result, these zone plates can be ideally designed to offer a time-bandwidth product (TBP) as large as desired, practically limited by the achievable temporal modulation bandwidth (limiting the temporal resolution) and the amount of dispersion needed in the target processing systems (limiting the temporal aperture). We numerically and experimentally demonstrate linear optical pulse compression by using temporal zone plates based on linear electro-optic temporal modulation followed by fiber-optics dispersion. In the pulse-compression experiment based on temporal phase zone plates, we achieve a resolution of ~25.5 ps over a temporal aperture of ~5.77 ns, representing an experimental TBP larger than 226 using a phase-modulation amplitude of only ~0.8π rad. We also numerically study the potential of these devices to achieve temporal imaging of optical waveforms and present a comparative analysis on the performance of different temporal intensity and phase zone plates.

OCIS codes: (070.1170) Analog optical signal processing; (320.5520) Pulse compression; (110.6915) Time imaging.

References and links

1. T. Jannson and J. Jannson, "Temporal self-imaging effect in single-mode fibers," J. Opt. Soc. Am. **71**, 1373–1376 (1981).
2. Y. Kato, K. Mima, N. Miyanaga, S. Arinaga, Y. Kitagawa, M. Nakatsuka, and C. Yamanaka, "Random phasing of high-power lasers for uniform target acceleration and plasma-instability suppression," Phys. Rev. Lett. **53**(11), 1057–1060 (1984).
3. B. H. Kolner, *Broadband Optical Modulators* (CRC Press, 2011), Chap. 19.
4. B. H. Kolner, "Generalization of the concepts of focal length and f-number to space and time," J. Opt. Soc. Am. A **11**(12), 3229–3234 (1994).
5. C. V. Bennett, R. P. Scott, and B. H. Kolner, "Temporal magnification and reversal of 100 Gb/s optical data with an up-conversion time microscope," Appl. Phys. Lett. **65**(20), 2513–2515 (1994).
6. R. Salem, M. A. Foster, A. C. Turner, D. F. Geraghty, M. Lipson, and A. L. Gaeta, "Optical time lens based on four-wave mixing on a silicon chip," Opt. Lett. **33**(10), 1047–1049 (2008), http://www.opticsinfobase.org/ol/abstract.cfm?URI=ol-33-10-1047.
7. B. H. Kolner, "Space-time duality and the theory of temporal imaging," IEEE J. Quantum Electron. **30**(8), 1951–1963 (1994).
8. J. Wigmore and D. Grischkowsky, "Temporal compression of light," IEEE J. Quantum Electron. **14**(4), 310–315 (1978).
9. J. Bjorkholm, E. Turner, and D. Pearson, "Conversion of cw light into a train of subnanosecond pulses using frequency modulation and the dispersion of a near-resonant atomic vapor," Appl. Phys. Lett. **26**(10), 564–566 (1975).

#189054 - $15.00 USD Received 1 May 2013; revised 27 Jun 2013; accepted 28 Jun 2013; published 5 Jul 2013

10. J. van Howe, J. Hansryd, and C. Xu, "Multiwavelength pulse generator using time-lens compression," Opt. Lett. **29**(13), 1470–1472 (2004).
11. M. Kauffman, W. Banyai, A. Godil, and D. Bloom, "Time-to-frequency converter for measuring picosecond optical pulses," Appl. Phys. Lett. **64**(3), 270–272 (1994).
12. M. A. Foster, R. Salem, D. F. Geraghty, A. C. Turner-Foster, M. Lipson, and A. L. Gaeta, "Silicon-chip-based ultrafast optical oscilloscope," Nature **456**(7218), 81–84 (2008).
13. T. T. Ng, F. Parmigiani, M. Ibsen, Z. Zhang, P. Petropoulos, and D. J. Richardson, "Compensation of linear distortions by using XPM with parabolic pulses as a time lens," IEEE Photon. Technol. Lett. **20**(13), 1097–1099 (2008).
14. R. Llorente, R. Clavero, and J. Marti, "Performance analysis of polarimetric PMD monitoring by real-time optical Fourier transformers," IEEE Photon. Technol. Lett. **18**(12), 1383–1385 (2006).
15. R. P. Scott, N. K. Fontaine, D. J. Geisler, and S. Yoo, "Frequency-to-time-assisted interferometry for full-field optical waveform measurements with picosecond resolution and microsecond record lengths," IEEE Photon. J. **4**(3), 748–758 (2012).
16. M. A. Muriel, J. Azaña, and A. Carballar, "Real-time Fourier transformer based on fiber gratings," Opt. Lett. **24**(1), 1–3 (1999), http://ol.osa.org/abstract.cfm?URI=ol-24-1-1.
17. B. H. Kolner, "The pinhole time camera," J. Opt. Soc. Am. A **14**(12), 3349–3357 (1997).
18. J. Azaña and M. A. Muriel, "Temporal self-imaging effects: theory and application for multiplying pulse repetition rates," IEEE J. Sel. Top. Quantum Electron. **7**(4), 728–744 (2001).
19. L. E. Munioz-Camuniez, V. Torres-Company, J. Lancis, J. Ojeda-Castaneda, and P. Andres, "Electro-optic time lens with an extended time aperture," J. Opt. Soc. Am. B **27**(10), 2110–2115 (2010).
20. M. T. Flores-Arias, L. Chantada, C. Bao, M. V. Pérez, and C. Gómez-Reino, "Temporal zone plate," J. Opt. Soc. Am. A **25**(12), 3077–3082 (2008).
21. R. W. Wood, "Zone-plate," in *Physical optics*, (The Macmillan Company, New York, 1934).
22. X. Huang, M. Wojcik, N. Burdet, I. Peterson, G. R. Morrison, D. J. Vine, D. Legnini, R. Harder, Y. S. Chu, and I. K. Robinson, "Quantitative X-ray wavefront measurements of Fresnel zone plate and KB mirrors using phase retrieval," Opt. Express **20**(21), 24038–24048 (2012), http://www.opticsinfobase.org/oe/abstract.cfm?uri=oe-20-21-24038.
23. Y. Wang, K. Kumar, L. Wang, and X. Zhang, "Monolithic integration of binary-phase fresnel zone plate objectives on 2-axis scanning micromirrors for compact microscopes," Opt. Express **20**(6), 6657–6668 (2012), http://www.opticsinfobase.org/oe/abstract.cfm?uri=oe-20-6-6657.
24. G. S. Waldman, "Variations on the Fresnel zone plate," J. Opt. Soc. Am. **56**(2), 215–218 (1966).
25. L. Rayleigh, "Wave Theory of Light," in *Encyclopedia Britannica, 9th ed.*, **24**, 429 (1888).
26. R. W. Wood, "LIII. Phase-reversal zone-plates, and diffraction-telescopes," The London, Edinburgh, and Dublin Philosophical Magazine and Journal of Science. **45**, 511-522 (1898).
27. J. Kirz, "Phase zone plates for x rays and the extreme uv," J. Opt. Soc. Am. **64**(3), 301–309 (1974).
28. L. F. Collins, "Diffraction theory description of bleached holograms," Appl. Opt. **7**(6), 1236–1237 (1968).
29. M. H. Horman, "Efficiences of zone plates and phase zone plates," Appl. Opt. **6**(11), 2011–2013 (1967).
30. C. E. Shannon, "Communication In The Presence Of Noise," Proc. IEEE **86**(2), 447–457 (1998).

1. Introduction

The space-time duality arises from the mathematical equivalence between paraxial diffraction in the spatial domain and dispersive propagation in the time domain [1–19]. Using the mature concepts of free-space Fourier optics, researchers have developed a wide variety of equivalent methods for temporal processing based on this general idea. Among many others, systems for temporal imaging [4–7], linear compression [8–10], time-to-frequency mapping [11, 12], and frequency-to-time mapping [13–16] of optical pulse waveforms have been realized by suitably combining dispersion and time lenses in the time domain, which are the temporal counterparts of diffraction and lenses in the spatial domain.

A time lens is conventionally implemented by imparting a quadratic phase shift, or linear frequency chirp, across a signal (e.g. a pulse) in the temporal domain. It can be realized by linear [7–11] or nonlinear [5, 6, 12, 13] processes. In particular, a linear time lens can be practically implemented by using an electro-optic phase modulator (EOPM) driven by a sinusoidal-like RF signal [1–5, 7–11]. Linear time lenses offer important practical advantages over nonlinear implementations, including wavelength-preserving operation, lower power consumption, and easier reconfiguration [19]. A main figure of merit of a time lens is its time-bandwidth product (TBP), namely the product of its temporal aperture (typically defining the maximum duration of the signal under analysis) and its frequency bandwidth (typically defining the system temporal resolution). In conventional linear time-lens methods, there is a tradeoff between the system temporal aperture and frequency bandwidth, and in particular, the TBP $\sim\Gamma_0/2\pi$ is limited by the achievable phase-modulation amplitude peak Γ_0 [3, 4].

#189054 - $15.00 USD Received 1 May 2013; revised 27 Jun 2013; accepted 28 Jun 2013; published 5 Jul 2013

Unfortunately, a high phase-modulation amplitude, e.g. exceeding 10π [10, 12, 19], is hard to achieve in a practical EOPM device.

The temporal equivalent of a spatial Fresnel zone plate (FZP) has been proposed as an alternative to conventional time lenses [20]. However, this scheme is greatly limited by the need to implement a temporal modulation with an ideally infinite bandwidth. In this communication, we generalize this concept into more practical and effective "temporal zone plate" implementations. "Temporal zone plates" are defined as the time-domain equivalents of spatial zone plates [20–29]. We consider two kinds of schemes, based on intensity and phase modulation, respectively referred to as "temporal intensity zone plates" and "temporal phase zone plates". Two different sub-classes of temporal zone plates are additionally introduced and investigated for each of the two considered cases (phase and intensity modulated systems, respectively). We show how in the proposed temporal zone plate schemes, the temporal aperture can be designed to be as long as desired without affecting the time-lens frequency bandwidth. As such, temporal zone plates can directly overcome the severe TBP limitations of present linear time-lens methods. In practice, the temporal aperture will be limited by the amount of dispersion needed in the target processing system, whereas the time-lens frequency bandwidth is limited by the bandwidth of the modulating signal.

Temporal intensity zone plates are here numerically and experimentally demonstrated for linear optical pulse compression using an electro-optic intensity modulator (EOIM). Using an electronic waveform generated from a 24 Gsamples/s arbitrary waveform generator (AWG), we achieve an experimental temporal resolution of ~47.9 ps over a temporal aperture of ~1.88 ns, representing a TBP > 39. Temporal phase zone plates are also experimentally demonstrated for linear optical pulse compression using an EOPM. In this later case, using a phase-modulation amplitude limited to $\sim 0.8\pi$ rad and an electronic waveform generated from a 24 Gsamples/s AWG, we achieve an experimental temporal resolution of ~25.5 ps over a temporal aperture of ~5.77 ns, representing a TBP > 226. Notice that a TBP of 39 (or 226) is difficult to achieve with conventional linear electro-optic time-lens methods, since an extremely high phase-modulation amplitude exceeding 39π (or 226π) rad would then be required [3, 4, 10]. Correspondingly, the needed drive-voltage amplitude should be as high as $39V_\pi$ (or $226V_\pi$), where V_π is the phase-modulator switching voltage. In our experiments, a much lower drive-voltage amplitude of only $\sim V_\pi$ is used. We also numerically demonstrate the potential of temporal intensity and phase zone plates to create temporal imaging systems.

This paper discusses fundamental and practical considerations of temporal zone plates. Section 2 provides the principle, numerical simulations and experiments for temporal intensity zone plates. In section 3, the principle, numerical simulations and experiments for temporal phase zone plates are reported. Section 4 describes the temporal imaging performance of temporal intensity and phase zone plates, whereas the main conclusions of this work are summarized in Section 5.

2. Temporal intensity zone plates

In this section, we derive analytical expressions for temporal intensity zone plates. Then we prove our theory by means of numerical simulations and experiments.

2.1 Principle of operation

The first zone plate, called a FZP, was discovered by Lord Rayleigh in 1871 [21]. It was made out of a plate with alternating transmitting and opaque concentric rings with diameters being proportional to the square roots of the orders of the rings, as illustrated in Fig. 1(a). This configuration ensures that all the light passing through the plate, around the target wavelength, have a phase between ϕ_0 to $\phi_0 + \pi$ at the focus, where ϕ_0 is a constant phase. In this way, the light at the focus is enhanced as a result of constructive interference. Note that the modulation profile consists of many rectangular shapes, which may not be easy to be implemented in practice. Therefore, Gabor zone plates (GZPs) were subsequently proposed to facilitate the device realization [24]. GZPs are implemented by replacing the rectangular shapes with approximately sinusoidal shapes. Mathematically, the amplitude-transmittance

#189054 - $15.00 USD Received 1 May 2013; revised 27 Jun 2013; accepted 28 Jun 2013; published 5 Jul 2013

functions of FZPs and GPZs are defined as $A_F(x) = 1/2 + (1/2)\ \mathrm{sgn}[\cos(\gamma x^2)]$ and $A_G(x) = 1/2 + (1/2)\cos(\gamma x^2)$, respectively, where γ is a constant, and $\mathrm{sgn}[\cos(\gamma x^2)] = \pm 1$ depends on the sign of $\cos(\gamma x^2)$. As illustrated in Fig. 1, the time-domain analogs of these spatial zone plates would be temporal intensity modulation devices, which have the same amplitude-transmittance functions but as a function of the time variable (t), particularly,

$$A_F(t) = 1/2 + (1/2)\,\mathrm{sgn}\left[\cos\left(at^2\right)\right], \tag{1}$$

$$A_G(t) = 1/2 + (1/2)\cos\left(at^2\right), \tag{2}$$

for $-\Delta t/2 < t < \Delta t/2$, where Δt is the temporal aperture, and a/π is the modulation frequency chirp, which is related with the time-lens frequency chirp. Using a Fourier series, the amplitude-transmittance functions of the temporal FZP and the temporal GZP in Eqs. (1) and (2) can be re-written as

$$A_F(t) = \sum_{n=-\infty}^{\infty}\left[\sin\left(n\pi/2\right)/n\pi\right]\exp\left(jnat^2\right), \tag{3}$$

$$A_G(t) = \sum_{n=-1}^{1}\left(1/2 - n^2/4\right)\exp\left(jnat^2\right), \tag{4}$$

respectively. Noting that temporal quadratic phase structures can be interpreted as being equivalent to time lenses, the above equations confirm that these amplitude-transmittance functions are equivalent to a set of positive and negative time lenses with different focal times (i.e., each with a different frequency chirp, depending on the integer order n), plus a bias term. Considering the phase equation typically used for a time lens $\phi(t) = \omega_0 t^2/2f_T$, where ω_0 is the optical carrier frequency and f_T is the focal time, the focal time of the n-th term in any of the proposed temporal intensity zone plates is $f_{Tn} = \omega_0/2na$. Thus, the focal time is inversely proportional to the integer order n, or in other words, the time-lens frequency chirp increases linearly with the order n. In particular, the time-lens frequency chirp for the n-th order term is defined as na/π. It is also important to note that similarly to their spatial-domain counterparts, temporal intensity zone plates do not focus all the input light around the desired focal time, as illustrated in Fig. 1(b). The proportion of light focused by the n-th order term can be obtained by the square of its coefficient in the Fourier series [Eqs. (3) and (4)]. In particular, the light-collecting efficiencies (i.e., the proportion of focused light) around the n-th focal time for temporal FZP and GZP devices are

$$\eta_F = \left[\sin\left(n\pi/2\right)/n\pi\right]^2, \tag{5}$$

$$\eta_G = \left(1/2 - n^2/4\right)^2. \tag{6}$$

Clearly, for any of the two proposed implementations, the light-collecting efficiency quickly decreases with the order n.

#189054 - $15.00 USD Received 1 May 2013; revised 27 Jun 2013; accepted 28 Jun 2013; published 5 Jul 2013

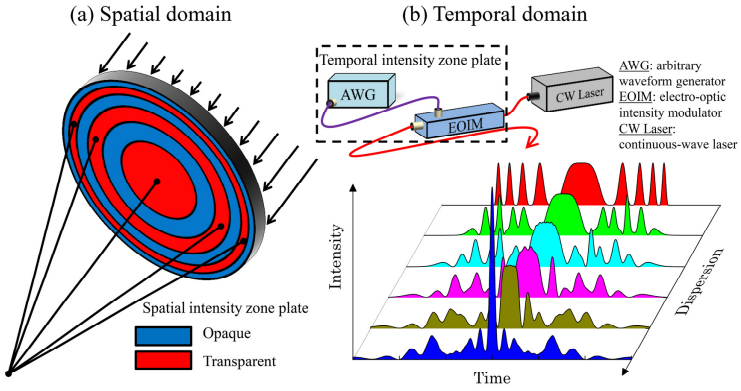

Fig. 1. Space-time duality. (a) Light focusing by a spatial (intensity) zone plate. (b) Pulse compression by a temporal intensity zone plate.

The proposed temporal intensity zone plates can be practically realized by using an EOIM, i.e. a conventional electro-optic Mach-Zehnder modulator biased at quadrature, which is driven by a modulating electronic waveform with a temporal profile defined as the square of the expression in Eqs. (1) or (2). In practice, the electronic waveforms can be obtained from a high-speed AWG. For a given chirp factor a, the temporal aperture must be limited due to finite bandwidth of the AWG. According to the Nyquist-Shannon sampling theorem [30], the sampling rate f_s of the AWG should be at least two times larger than the bandwidth of the electronic waveform. Consequently, the temporal apertures of temporal FZPs and GZPs must satisfy the following inequalities $\Delta t_F < f_s / 3.5|a|$ and $\Delta t_G < f_s\pi/|a|$, respectively. Notice that the total frequency bandwidth excursion produced by a quadratic phase $\phi(t) = nat^2$ along an aperture Δt is $\Delta f = |na|\Delta t/\pi$ [4]. This total bandwidth excursion determines the temporal resolution of the time-lens system. In particular, for the case of a temporal imaging system with a rectangular temporal aperture function, the temporal resolution ($\delta\tau$) is given by $\delta\tau = 1/\Delta f$ [4, 7]. Hence, the TBPs and temporal resolutions of temporal FZPs and GZPs are finally determined by the following inequalities

$$\delta\tau_F \geq 3.5\pi/|n| f_s, \tag{7}$$

$$\delta\tau_G \geq 1/|n| f_s. \tag{8}$$

$$TBP_F = \Delta t_F/\delta\tau_F \leq |n| f_s^2/12.6|a|\pi, \tag{9}$$

$$TBP_G = \Delta t_G/\delta\tau_G \leq |n|\pi f_s^2/|a|, \tag{10}$$

Equations (7) and (8) show that the temporal resolutions increase as $1/|n|f_s$. Nonetheless, according to Eqs. (5) and (6), most of the light in either a temporal FZP or a temporal GZP is focused in the order $|n| = 1$ and as a result, only these orders can be used in practical designs. Thus, as defined by Eqs. (7) and (8) for $|n| = 1$, the temporal resolution in any of these two implementations is directly limited by the modulating signal frequency bandwidth, in turn fixed by the AWG bandwidth. In addition, the temporal apertures, and corresponding TBPs in Eq. (9), are inversely proportional to the chirp factor $|a|$, and consequently, they can be made arbitrarily large by accordingly lowering down this factor. However, signal-processing systems are typically based on the combination of a time lens and dispersive elements [7, 10, 12, 13]. In these schemes, the time-lens frequency chirp is typically inversely proportional to the dispersion value in the system: a lower time-lens frequency chirp necessarily translates into the need for a higher amount of dispersion. Thus, the temporal apertures and TBPs of temporal intensity zone plates are ultimately limited by the amount of dispersion that can be practically introduced in the system. Finally, Eqs. (7)-(10) also show that temporal GZPs have

#189054 - $15.00 USD Received 1 May 2013; revised 27 Jun 2013; accepted 28 Jun 2013; published 5 Jul 2013

better TBPs and resolutions than temporal FZPs, which is associated with the fact that in practice, the sinusoidal profile of a GZP is easier to realize, i.e., it requires lower sampling rate, than the rectangular profile of a FZP. Thus, the experimental demonstrations reported in what follows focus on temporal GZPs.

2.2 Numerical simulations and experiments

Temporal GZPs are numerically and experimentally demonstrated, while temporal FZPs are numerically verified. A following brief comparison is then given.

2.2.1 Temporal Gabor zone plate

To demonstrate the introduced temporal intensity zone plate concept, we set up a linear optical pulse compression experiment based on 1st-order temporal GZPs. An illustration of the conducted experiment is shown in Fig. 2. Light from a continuous-wave (CW) laser at a wavelength of 1,550 nm is amplified and sent through a 40-GHz EOIM (V_π = 4.6 V), which is driven by the electronic waveforms generated by a 24 Gsamples/s AWG and amplified by a 12.5-GHz electronic amplifier. The modulated light is sent through a reflective linearly chirped fiber Bragg grating (LCFBG), which introduces a predominantly 1st-order dispersion over a bandwidth of ~0.5nm. After dispersion, the light is measured with a 45-GHz photo-detector coupled to an electronic sampling oscilloscope.

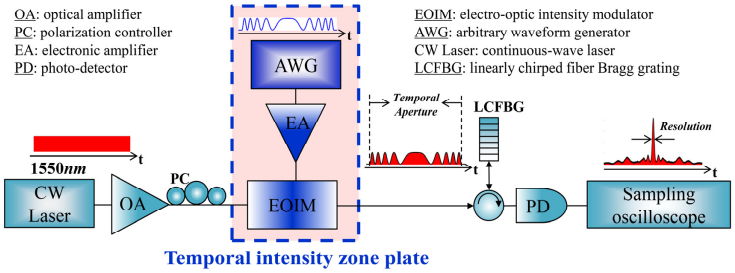

Fig. 2. Experimental scheme for linear optical pulse compression using the temporal GZP concept, with the terminology used in the text.

We characterized our system in two regimes of dispersion introduced by the LCFBG, which are 10000 ps/nm and 6667 ps/nm, respectively. The ideal optical intensity waveforms (green dotted curves), which are calculated by Eq. (2), are shown in Fig. 3. The slight distortions between the electronic modulation waveforms (blue dashed curves, directly measured with the same sampling oscilloscope, right vertical axis) and ideal optical waveforms are mainly due to the limited bandwidth of the AWG. A low drive-voltage amplitude of ~V_π is used. There is a good agreement between the electronic modulation waveforms and the measured optical waveforms (black solid curves). In the pulse compression experiments, the time-lens frequency chirp must be fixed to exactly compensate for the LCFBG dispersion. Thus, a lower chirp factor, $|a|$, corresponding to a longer aperture, is needed as the dispersion is increased. As a result, the temporal apertures for the two dispersion regimes demonstrated here are 1.88 ns and 1.22 ns, respectively.

#189054 - $15.00 USD Received 1 May 2013; revised 27 Jun 2013; accepted 28 Jun 2013; published 5 Jul 2013

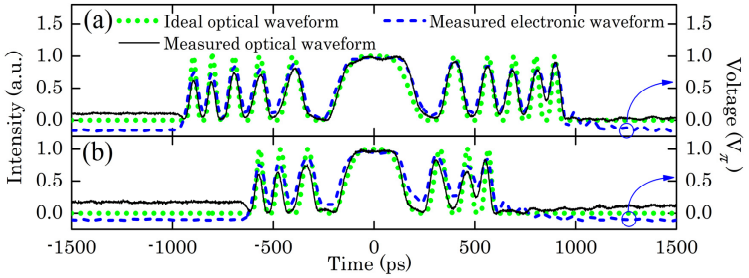

Fig. 3. Ideal optical waveforms (left vertical axis), measured electronic waveforms (right vertical axis), and measured optical waveforms (left vertical axis) for temporal intensity modulation in the implemented temporal GZPs when the used dispersion values are (a) 10000 ps/nm and (b) 6667 ps/nm, respectively. All optical waveforms are represented in normalized units.

Figure 4 shows the spectra of the CW light (red dotted curves) and the modulated light (black solid curves). After the intensity modulation, the spectra are effectively broadened. In particular, the modulated light in Fig. 4(a) has a larger spectrum than that of Fig. 4(b). Therefore, the output with shorter pulse width will be obtained in the first experiment. Figure 5 shows the resulting compressed optical pulses measured at the system output. As predicted in Fig. 4, for the two dispersion values, the full width at half maximum (FWHM) of the experimentally measured compressed pulses are 47.9 ps and 57.6 ps, respectively, whereas the corresponding ideal values calculated through numerical simulations are 45.2 ps and 48.6 ps, respectively. The excellent agreement for the first experiment clearly confirms our theoretical predictions, while the larger distortion in the second experiment is mainly attributed to the fact that the corresponding modulating electronic waveform deviates more significantly from the ideal modulation, as shown in Fig. 3. There is also a fairly good agreement between the simulation and experiment concerning the temporal side-lobe structures, which are mainly induced by the presence of undesired-order (n = 0 and –1) focal terms.

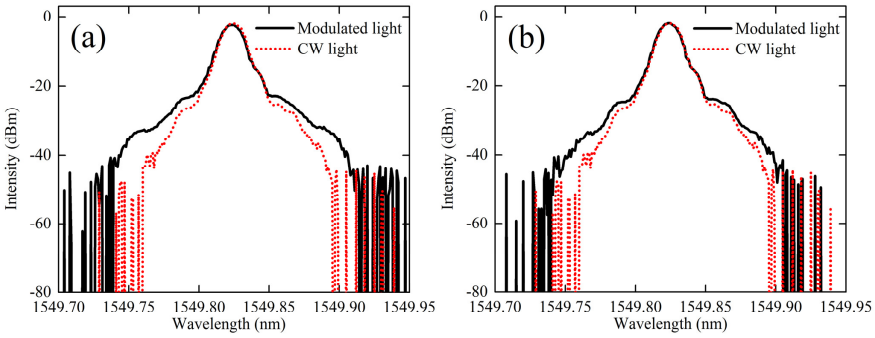

Fig. 4. Spectra of the CW light and the modulated light for two regimes in which dispersion values of (a) 10000 ps/nm and (b) 6667 ps/nm are used, respectively. The spectra are measured by an optical spectrum analyzer, which has a resolution of 0.01 nm.

#189054 - $15.00 USD Received 1 May 2013; revised 27 Jun 2013; accepted 28 Jun 2013; published 5 Jul 2013

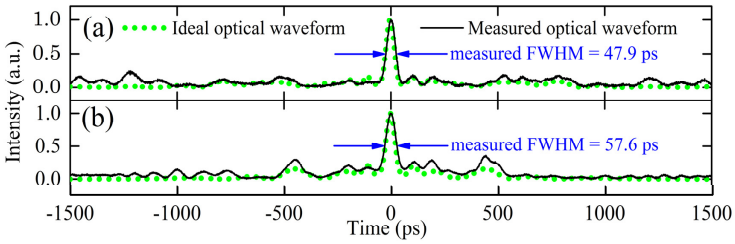

Fig. 5. Temporally compressed intensity pulse waveforms in the ideal case and experiment using temporal GZPs when the used dispersion values are (a) 10000 ps/nm and (b) 6667 ps/nm, respectively. All waveforms are represented in normalized units.

2.2.2 Temporal Fresnel zone plate

The realization of a temporal FZP needs a modulating signal with quite a large bandwidth, ideally infinite (see section 2.2.3), which is difficult to realize in practice. As a result, we demonstrate the potential of pulse compression using 1st-order temporal FZPs through numerical simulations. The system scheme is the same as the one shown in Fig. 2. In the numerical simulation, we also characterized our system in two regimes of dispersion, which are 10000 ps/nm and 6667 ps/nm, respectively. To fully evaluate the performance of the temporal FZP, a comparison of pulse compression based on a temporal FZP and that based on a temporal GZP is illustrated in Fig. 6. The intensity-modulation profiles of temporal FZPs (red solid curves) and temporal GZPs (blue dashed curves) are shown in Fig. 6(a) and 6(b). These profiles are defined by Eqs. (1) and (2), respectively. The temporal intensity profiles and spectra of the corresponding output compressed pulses are shown in Fig. 6(c)-6(f). For the temporal FZPs shown in Fig. 6(a) and 6(b), the peak powers of the outputs [red solid curves in Fig. 6(c) and 6(d)] are 7 and 4.85 times larger than the peak power of the input CW light, respectively. As predicted in Eqs. (5) and (6), the temporal GZP suffers from a somewhat inferior light-collecting efficiency. In particular, for the temporal GZPs shown in Fig. 6(a) and 6(b), the peak powers of the outputs [blue dashed curves in Fig. 6(c) and 6(d)] are 4.8 and 3.5 times larger than the peak power of input CW light, respectively. Similar side-lobe structures in Fig. 6(c)-6(f) are induced by the presence of undesired-order focal terms.

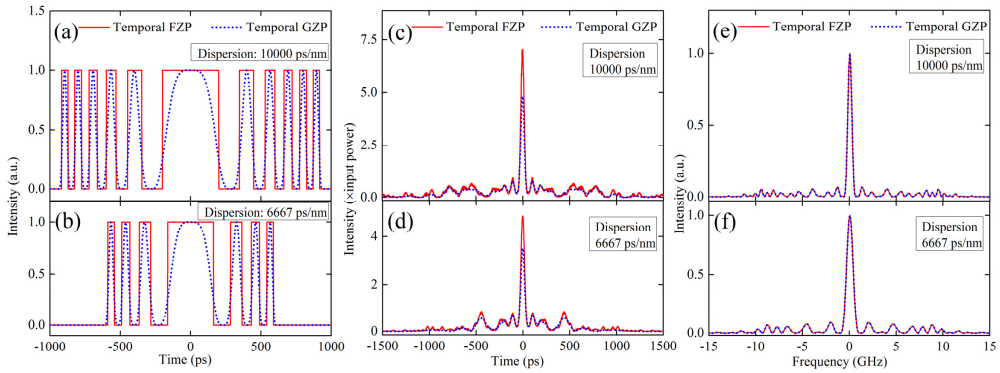

Fig. 6. The intensity-modulation profiles of temporal FZPs and temporal GZPs when the used dispersion values are (a) 10000 ps/nm and (b) 6667 ps/nm, respectively. The output compressed pulses in (c), (e) and (d), (f) correspond to (a) and (b), respectively.

2.3 Brief comparison between the two intensity zone plate concepts

As the intensity-modulation profiles for two intensity zone plates are different, different modulation bandwidth will be needed. Figure 7(a), 7(c) and 7(b), 7(d) show the spectra of the modulating signals shown in Fig. 6(a) and 6(b), respectively. In particular, the modulation

#189054 - $15.00 USD Received 1 May 2013; revised 27 Jun 2013; accepted 28 Jun 2013; published 5 Jul 2013

bandwidth for temporal GZP is limited, while the modulation bandwidth for temporal FZP is ideally infinite, as shown in Fig. 7(c) and 7(d). Therefore, a temporal GZP is easier to realize than a temporal FZP in terms of modulation bandwidth.

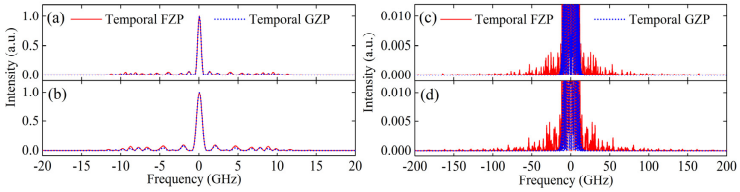

Fig. 7. The spectra of the modulating signals shown in Fig. 6. Figure 7(a) and 7(b) correspond to Fig. 6(a) and 6(b), respectively. Figure 7(c) and 7(d) show a zoom around the bottom of Fig. 7(a) and 7(b), respectively.

According to Eqs. (5) and (6), most of the light in either a temporal FZP or a temporal GZP is focused in the order $|n| = 1$. In particular, the light-collecting efficiencies of 1st-order temporal FZP and 1st-order temporal GZP are $1/\pi^2$ and 1/16, respectively. Thus, a temporal GZP suffers from a slightly inferior light-collecting efficiency.

Apart from these differences, both the temporal GZP and the temporal FZP can offer large temporal apertures by the use of large dispersion. The resolutions of these temporal intensity zone plates are both directly limited by the bandwidth of the modulating signals. Moreover, the relatively low light-collecting efficiency and large background may limit the range of applications of these temporal intensity zone plates.

3. Temporal phase zone plates

In this section, we derive analytical expressions for temporal phase zone plates. Then we prove our theory by means of numerical simulations and experiments.

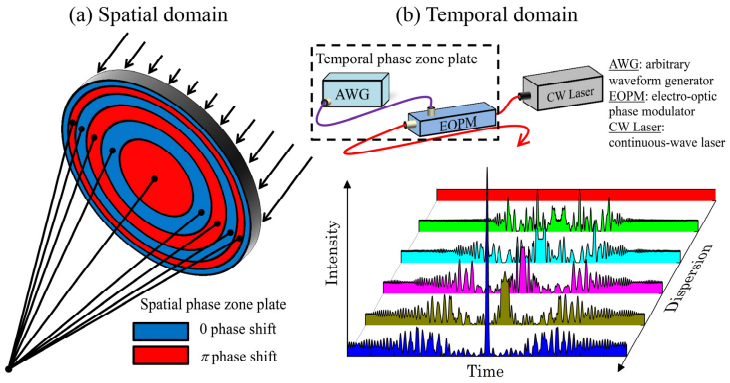

Fig. 8. Space-time duality. (a) Light focusing by a spatial phase zone plate. (b) Pulse compression by a temporal phase zone plate.

3.1 Principle of operation

To overcome the two difficulties of a spatial (intensity) zone plate, i.e., low light-collecting efficiency and high background, Lord Rayleigh proposed the phase-reversal zone plate in 1888 [25] and Wood demonstrated its advantages over Fresnel zone plates 10 years later [26]. In the spatial domain, there are two kinds of phase zone plates, called as Rayleigh-Wood phase reversal zone plates (RWZPs) and Gabor phase-shift zone plates (GPZPs) [25–27]. Specifically, the RWZP consists of a series of concentric ring-shaped zones, which are shown in Fig. 8(a). The path from a point on one certain zone to the focus has a variable range of half a wavelength. By adding or subtracting a π rad shift across the light going through

#189054 - $15.00 USD Received 1 May 2013; revised 27 Jun 2013; accepted 28 Jun 2013; published 5 Jul 2013

alternate zones, the wavefield at the focus will be enhanced by constructive interference. The GPZP is also a spatial phase modulation device. Differently, the GPZP has an approximately sinusoidal modulation profile. Although the GPZP has a somewhat inferior light-collecting efficiency compared to the RWZP, it is easier to realize in practice [27]. Mathematically, the phase-modulation profiles of these two zone plates can be respectively expressed as $\phi_{RW}(x) = \pi/2 + (\pi/2)\mathrm{sgn}[\cos(\gamma x^2)]$ and $\phi_{GP}(\mathrm{x}) = \Gamma_0'\cos(\gamma x^2)]$ where γ is a constant, Γ_0' is the phase-modulation amplitude, and $\mathrm{sgn}[\cos(\gamma x^2)] = \pm 1$ depends on the sign of $\cos(\gamma x^2)$. Therefore, as illustrated in Fig. 8, the time-domain analogs of these spatial phase zone plates would be temporal phase modulation devices introducing equivalent phase shifts but along the time axis (t), particularly,

$$\phi_{RW}(t) = \pi/2 + (\pi/2)\,\mathrm{sgn}\left[\cos\left(at^2\right)\right], \tag{11}$$

$$\phi_{GP}(t) = \Gamma_0 \cos\left(at^2\right) \tag{12}$$

for $-\Delta t/2<t<\Delta t/2$, where Δt is the temporal aperture, a/π is the phase-modulation frequency chirp, and Γ_0 is the phase-modulation amplitude. Using a Fourier series and a Bessel function identity [28, 29], the instantaneous phase transformations of the temporal RWZP and the temporal GPZP in Eqs. (11) and (12) can be re-written as

$$H_{RW}(t) = \exp\left[j\phi_{RW}(t)\right] = 2\sum\nolimits_{n=-\infty,n\neq 0}^{\infty}\left[\sin\left(n\pi/2\right)/n\pi\right]\exp\left(jnat^2\right), \tag{13}$$

$$H_{GP}(t) = \exp\left[j\phi_{GP}(t)\right] = \sum\nolimits_{n=-\infty}^{\infty} j^n J_n\left(\Gamma_0\right)\exp\left(jnat^2\right), \tag{14}$$

respectively, where J_n is the n-th order Bessel function. The above equations confirm that these phase-modulation functions are equivalent to a set of positive and negative time lenses at different focal times, i.e., each with a different frequency chirp, depending on the integer order n. Comparing the above instantaneous phase transformations with the phase of a time lens $\phi(t) = \omega_0 t^2/2f_T$, in which ω_0 is the optical carrier frequency, the focal time of the n-th term in any of the proposed temporal phase zone plates is $f_{Tn} = \omega_0/2na$. Thus, the focal time is inversely proportional to the integer order n, or in other words, the time-lens frequency chirp, defined as na/π, increases linearly with the order n. Note that similarly to their spatial-domain counterparts, temporal phase zone plates do not focus all the input light around the desired focal time, as illustrated in Fig. 8(b). The proportion of light focused by n-th order term can be obtained by the square of its coefficient in the above series expansions [Eqs. (13) and (14)]. In particular, the light-collecting efficiencies (i.e., the proportion of focused light) around the n-th focal time for temporal RWZP and temporal GPZP devices are

$$\eta_{RW} = 4\left[\sin\left(n\pi/2\right)/n\pi\right]^2, \tag{15}$$

$$\eta_G = \left[J_n\left(\Gamma_0\right)\right]^2. \tag{16}$$

Specifically, the light-collecting efficiency of a temporal GPZP is a slowly decaying periodic function of the phase-modulation amplitude, which is shown in Fig. 9(a). Therefore, for a temporal GPZP of any prescribed order $|n|\neq 0$, there is an optimum phase-modulation amplitude, as indicated by the arrows in Fig. 9(a), which ensures that the highest light-collecting efficiency is achieved for the target order while lowering the energy focused to other terms. The optimum efficiencies of temporal GPZPs and temporal RWZPs are shown in Fig. 9(b). The temporal RWZP has a higher light-collecting efficiency than the temporal GPZP when the order $|n|$ is 1. But for higher orders $|n|>1$, temporal GPZPs have much higher light-collecting efficiency than temporal RWZPs.

#189054 - $15.00 USD Received 1 May 2013; revised 27 Jun 2013; accepted 28 Jun 2013; published 5 Jul 2013

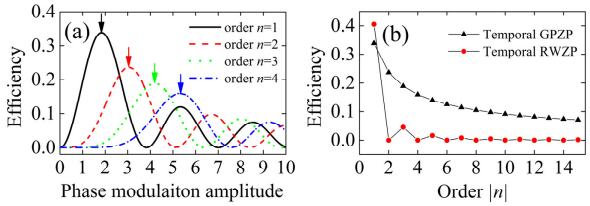

Fig. 9. (a) The light-collecting efficiency of temporal GPZP. The optimum phase-modulation amplitude for each order n is indicated by arrows. (b) The light-collecting efficiency of temporal GPZP and temporal RWZP, respectively.

A temporal phase zone plate can be practically realized by using an EOPM, which is driven by electronic waveforms with the profiles defined in Eqs. (11) and (12). In practice, the electronic waveforms can be obtained from a high-speed arbitrary waveform generator (AWG). Similarly to temporal intensity zone plates, for a given phase-modulation frequency-chirp factor a, the temporal aperture must be limited due to the finite frequency bandwidth of the AWG. Particularly, the temporal apertures of temporal RWZPs and temporal GPZPs must satisfy $\Delta t_{RW} < f_s/3.5|a|$ and $\Delta t_{GP} < f_s\pi/|a|$, respectively. As for the intensity zone plate analysis, the time-lens temporal resolution ($\delta\tau$) is estimated as $\delta\tau = 1/\Delta f$ [4, 7], where $\Delta f = |na|\Delta t/\pi$ is the total frequency bandwidth induced by a quadratic phase $\phi(t) = nat^2$ along an aperture Δt. The TBPs and temporal resolutions of temporal RWZPs and temporal GPZPs are finally limited by the following inequalities

$$\delta\tau_{RW} \geq 3.5\pi/|n|f_s, \tag{17}$$

$$\delta\tau_{GP} \geq 1/|n|f_s. \tag{18}$$

$$TBP_{RW} = \Delta t_{RW}/\delta\tau_{RW} \leq |n|f_s^2/12.6|a|\pi, \tag{19}$$

$$TBP_{GP} = \Delta t_{GP}/\delta\tau_{GP} \leq \pi|n|f_s^2/|a| \tag{20}$$

Equations (17) and (18) show that the temporal resolutions increase as $1/|n|f_s$. In addition, the temporal apertures, and corresponding TBPs, are inversely proportional to the chirp factor $|a|$, and consequently, they can be made arbitrarily large by accordingly lowering down this factor. Considering again that the time-lens frequency chirp is typically inversely proportional to the dispersion value in the system, the temporal apertures and TBPs of temporal phase zone plates are similarly limited by the amount of dispersion that can be practically introduced in the system. Equations (17)-(20) also show that temporal GPZPs have better TBPs and resolutions than temporal RWZPs, which is associated with the fact that in practice, the sinusoidal profile of a GPZP is easier to realize, i.e., it requires less modulation bandwidth, than the rectangular profile of a RWZP. Moreover, temporal GPZPs offer a significantly larger light-collecting efficiency for order $|n|>1$, as shown in Fig. 9(b). Thus, our experimental demonstrations focus on temporal GPZPs.

3.2 Numerical simulations and experiments

Temporal GPZPs are numerically and experimentally demonstrated, while temporal RWZPs are numerically verified. A following brief comparison is then given.

3.2.1 Temporal Gabor phase-shift zone plate

To demonstrate the introduced temporal phase zone plate concept, we set up a linear optical pulse compression experiment, in which 1st-order, 2nd-order, and 3rd-order temporal GPZPs are used. Figure 10 shows the linear optical pulse compression scheme. Light from a continuous-wave (CW) laser at a wavelength of 1,550 nm is amplified and sent through a 25-GHz EOPM (V_π = 3.8 V), which is driven by the electronic waveforms generated by a 24

#189054 - $15.00 USD Received 1 May 2013; revised 27 Jun 2013; accepted 28 Jun 2013; published 5 Jul 2013

Gsamples/s AWG and amplified by a 12.5-GHz electronic amplifier. The phase modulated light is sent through a reflective linearly chirped fiber Bragg grating (LCFBG), which introduces a predominantly 1st-order dispersion of 10,000 ps/nm over a bandwidth of ~0.5nm. After dispersion, the light is detected by a 500-GHz optical sampling oscilloscope.

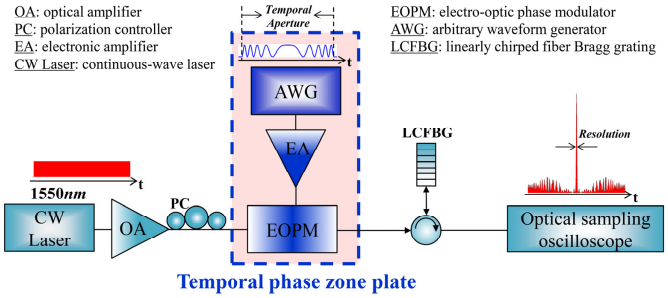

Fig. 10. Experimental scheme for linear optical pulse compression using the GPZP concept.

According to Eq. (16), for orders n = 1, 2, 3, the optimal phase-modulation amplitudes are respectively 1.84 rad, 3.05 rad, and 4.2 rad, which correspond to light-collecting efficiencies of 33.9%, 23.7%, and 18.9%, respectively. Limited by the available electronic amplifier (maximum voltage amplitude ~$0.8V_\pi$), a phase-modulation amplitude of only $\Gamma_0 \leq 0.8\pi$ is applied in all the reported experiments. The ideal modulating electronic waveforms, which are defined according to the target phase modulation profiles [Eq. (12)] considering the defined maximum voltage amplitude, are shown in Fig. 11 for 1st-order, 2nd-order, and 3rd-order temporal GPZPs (thick green curves). The measured electronic waveforms (thin blue curves in Fig. 11), as generated by the AWG, are slightly distorted mainly due to the limited bandwidth of the AWG. In the pulse compression experiments, the time-lens frequency chirp must be fixed to exactly compensate for the LCFBG dispersion. Thus, a lower $|a|$ is needed as the order n is increased. As a result, the temporal apertures, which are 1.88 ns, 3.85 ns, and 5.77 ns, respectively, increase as the order n increases from 1 to 3.

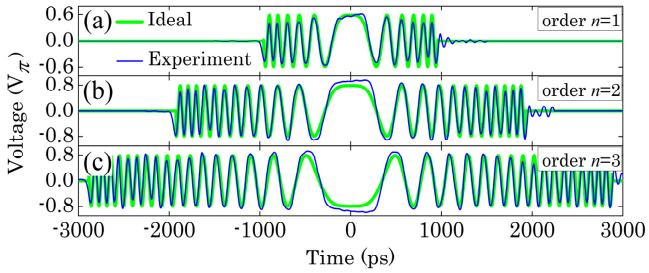

Fig. 11. Ideal and experimentally measured electronic waveforms for temporal phase modulation in the implemented temporal GPZPs for orders (a) n = 1, (b) n = 2, and (c) n = 3.

Figure 12 shows the spectra of the CW light (red dotted curves) and the modulated light (black solid curves). After the phase modulation, the spectra are effectively broadened. The phase-modulated light has a larger spectrum than intensity-modulated light, as shown in Fig. 4 and Fig. 12. The reason for this is the light-collecting efficiency of the temporal phase zone plate is higher. As predicted by Eq. (18), a higher order with the same sampling rate translates into an improved temporal resolution. In particular, we estimate that the FWHM of the compressed temporal pulses for the orders n = 1, 2, 3 should ideally be 36.5 ps, 17.8 ps, 13.3 ps, respectively, as shown in Fig. 13 (thick green solid curves). Deviations from these predictions are expected based on the described distortions in the practical temporal phase modulation profiles. The compressed pulse waveforms obtained in the experiments (thin blue solid curves) are in fairly good agreement with those calculated through numerical

#189054 - $15.00 USD Received 1 May 2013; revised 27 Jun 2013; accepted 28 Jun 2013; published 5 Jul 2013

simulations (red dotted curves), in which the deviations in the modulating electronic waveform and the bandwidth constraint of the EOPM are considered. For the cases of order n = 1, 2, 3, the FWHM of the compressed temporal pulses in the experiments are 38.6 ps, 23.9 ps, and 25.5 ps, respectively, and the corresponding values obtained in the simulations are 40.8 ps, 22 ps, and 23.6 ps, respectively. These results indicate that deviations in the phase modulating profiles have a more detrimental effect on the performance of higher-order focal terms. There is also a good agreement between the simulations and experiments concerning the temporal side-lobe structures outside the compressed pulse window, which are mainly induced by the presence of input light outside the time-lens aperture and the light collected into different focal times. These side-lobe structures can be additionally reduced by temporally filtering out the light beyond the aperture.

In the reported experiments, the power of the CW laser is 7.94 dBm (6.2 mW). As a result of the large loss induced by the EOPM (2.34 dB) and the LCFBG (10.96 dB), we used an optical amplifier, as shown in Fig. 10. The average powers of the output was measured (by a power meter) to be 1.22 dBm (1.3 mW) in all the reported experiments. The peak power of the outputs for the order n = 1, 2, 3 are directly measured (by the optical sampling oscilloscope) to be 11.46 dBm (14 mW), 14.31 dBm (27 mW), and 14.15 dBm (26 mW), respectively. The light-collecting efficiency can be estimated as the ratio of output-energy in the main lobe (estimated from the measured peak power and duration of the compressed pulse) versus output-energy during the temporal aperture (estimated from the measured output average power and duration of the aperture). Assuming that the main lobe has a Gaussian-like shape, the light-collecting efficiencies for the orders n = 1, 2, 3 were estimated to be 23.5%, 14.8%, and 9.4%, respectively. As expected, the light-collecting efficiency decreases as the order is increased. Notice also that the light-collecting efficiency into the order of interest could be further optimized by properly selecting the phase-modulation amplitude [see Fig. 9(a)]. For the sake of convenience, this optimization was not carried out in the experiments reported here.

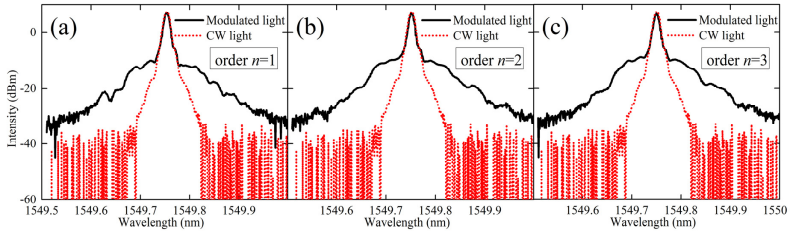

Fig. 12. Spectra of the CW light and the light modulated by temporal GPZPs for orders (a) n = 1, (b) n = 2, and (c) n = 3. The spectra are measured by an optical spectrum analyzer, which has a resolution of 0.01 nm.

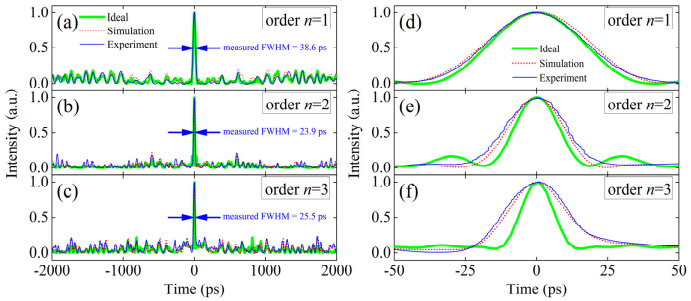

Fig. 13. Temporally compressed intensity waveforms in the ideal case, simulation, and experiment using temporal GPZPs of orders (a) n = 1, (b) n = 2, and (c) n = 3. (d)-(f) show a closer view of the compressed optical pulses in (a)-(c). All waveforms are represented in normalized units.

#189054 - $15.00 USD Received 1 May 2013; revised 27 Jun 2013; accepted 28 Jun 2013; published 5 Jul 2013

3.2.2 Temporal Rayleigh-Wood phase reversal zone plate

As high-speed rectangular shapes are difficult to realize in a practical experiment, we numerically demonstrate pulse compression based on temporal RWZPs, where orders n = 1, 2, 3 are used. The system scheme is the same as the one shown in Fig. 10. To fully demonstrate the performance of the temporal RWZP, a comparison of pulse compression based on the temporal RWZP and that based on the temporal GPZP is illustrated in Fig. 14. The phase-modulation profiles of temporal RWZPs (red solid curves) and temporal GZPs (blue dotted curves) are shown in Fig. 14(a)-14(c). These profiles are directly calculated from the analytical expressions in Eqs. (11) and (12). Note that the constant phase $\pi/2$ in Eq. (11) is omitted here. To optimize the light-collecting efficiencies, the optimal phase-modulation amplitudes for 1st-order, 2nd-order, and 3rd-order temporal GPZPs are 1.84 rad, 3.05 rad, and 4.2 rad, respectively. Differently, the phase-modulation amplitude for a temporal RWZP of any order is $\pi/2$, and thus the light-collecting efficiency for a temporal RWZP is independent of the phase-modulation amplitude, as shown in Fig. 9. The output compressed pulses corresponding to Fig. 14(a)-14(c) are shown in Fig. 14(d)-14(f), respectively. For temporal RWZPs of orders n = 1 and 3, the peak powers of the outputs (red solid curves) are 19 and 11.8 times larger than the average power of the input CW light, respectively. For temporal RWZPs of orders n = 2, there is no output compressed pulse [Fig. 14(e)] because the light-collecting efficiency is zero, as predicted by Eq. (15). For temporal GZPs of orders n = 1, 2, 3, the peak powers of the outputs (blue dotted curves) are 19, 58.5, and 102.5 times larger than the average power of the input CW light, respectively. Notice that these simulations do not take into consideration the passive losses in the modulation and dispersion devices. These results confirm that although temporal GPZPs suffer from limited light-collecting efficiency, they are potentially interesting for high-energy pulse generation by acting over longer input signal durations (higher input signal energies). For this purpose, the passive losses of the phase modulation and dispersive processes should be minimized.

To give some more details on the side-lobe structure of the compressed pulses, the normalized spectra of the output compressed pulses are shown in the right sets of Fig. 14(d)-14(f). Any of these spectra includes a main lobe with a Gaussian-like profile and some side-lobes. The resulting spectra are thus similar to those shown in Fig. 6(e) and 6(f) for the temporal intensity zone plates, except that the side-lobes have less energy in the phase zone plate cases. Therefore, from the presented results, it can be inferred that temporal phase zone plates induce a lower background than their intensity-modulation counterparts in pulse compression schemes.

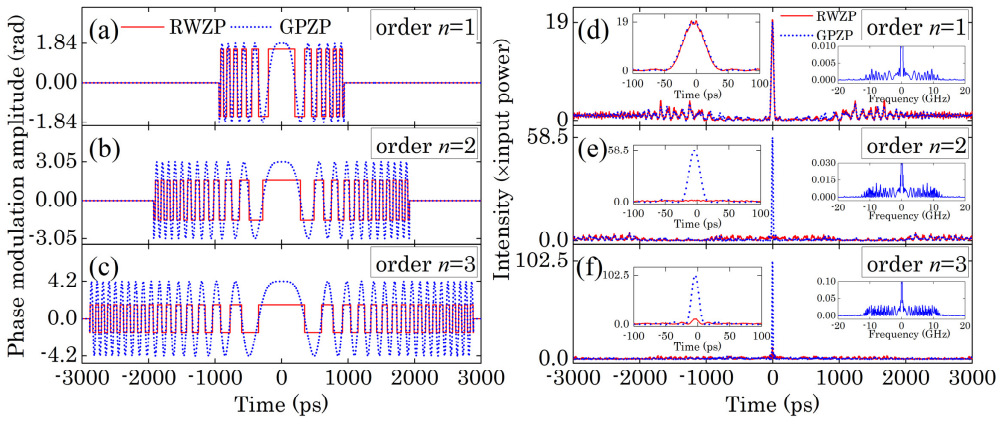

Fig. 14. Phase-modulation profiles for temporal RWZPs and temporal GPZPs of orders (a) n = 1, (b) n = 2, and (c) n = 3. The outputs in (d)-(f) correspond to (a)-(c), respectively. The left insets in (d)-(f) show a closer view of the output compressed optical pulses. The right insets in (d)-(f) are normalized spectra of the output compressed optical pulses.

#189054 - $15.00 USD Received 1 May 2013; revised 27 Jun 2013; accepted 28 Jun 2013; published 5 Jul 2013

3.3 Brief comparison between the two phase zone plate concepts

As discussed in subsection 2.3, the modulation bandwidth for a temporal GPZP is limited, while the modulation bandwidth for a temporal RWZP is ideally infinite. Therefore, a temporal GPZP is easier to realize than a temporal RWZP in terms of modulation bandwidth.

Although 1st-order temporal GPZP has a slightly lower light-collecting efficiency than 1st-order temporal RWZP, higher-order ($|n|>1$) temporal GPZPs have much higher light-collecting efficiency than temporal RWZPs, as shown in Fig. 9. It is important to note that higher-order temporal phase zone plates have larger temporal aperture and better temporal resolution.

Apart from these differences, both the temporal GPZP and the temporal FZP can offer large temporal apertures by the use of large dispersion. The resolutions of 1st-order temporal phase zone plates are both directly limited by the bandwidth of the modulating signals, while better resolution can be achieved by use of higher-order temporal GPZPs. Compared to temporal intensity zone plates, temporal phase zone plates have higher light-collecting efficiency and induce less background in pulse compression schemes.

4. Example of application for temporal imaging

In this subsection, we numerically provide several examples of temporal imaging based on temporal zone plates. A conventional temporal imaging system is shown in Fig. 15. In this system, a three-pulse sequence [1011] of unit amplitude Gaussian pulses is first dispersed, then linearly chirped (or quadratic phase shifted) by a time lens, and finally dispersed. The FWHM of any input pulse is 27.7 ps, while the repetition rate is 10GHz. When the imaging condition is satisfied, the output will be a replica of the input signal scaled in time [7]. In Fig. 15, the optical carrier frequency of input optical signal is 1550 nm, and the dispersion ϕ_1'' and ϕ_2'' are 10000 ps/nm and 2000 ps/nm, respectively. Thus the time scale is given by the ratio of the output dispersion to the input dispersion, i.e. $M = -2000/10000 \rightarrow M = -1/5$, which is shown in Fig. 15. Figure 16 shows the temporal intensity profiles (a-d) and spectra (e-h) of the output optical signals when the time lens in Fig. 15 is replaced with different temporal zone plates. Again, 2nd-order and 3rd-order temporal RWZPs cannot work as a result of their low light-collecting efficiency. Generally, time-scaled images are generated, although they are somewhat distorted. The FWHM of any output pulse is about 5.54 ps, while the repetition rate is 50GHz. The quality of the output images (b>c>d>a) is seen to be proportional to the light-collecting efficiency of the zone plates. However, according to the imaging condition [6, 7], the time-lens frequency chirp is approximately inversely proportional to the smaller dispersion value in the system (e.g. here it is 2000 ps/nm). Besides that a small time scale ($|M|<<1$) for temporal compression [or a large time scale ($|M|>>1$) for temporal magnification] is also desired. Thus the second dispersion amount in the system must be $1/|M|$ times (for temporal compression) or $|M|$ times (for temporal magnification), larger than this smaller dispersion. As a result, the temporal aperture and TBP of a temporal zone plate will be greatly limited by the achievable dispersion amount. For example, to achieve the performance in Fig. 16(a)-16(d), AWG sampling rates of 150 Gsamples/s, 150 Gsamples/s, 75 Gsamples/s, and 50 Gsamples/s will be needed, respectively.

Although temporal imaging can be implemented by temporal zone plates, the temporal apertures and TBPs will be ultimately restricted by the achievable dispersion. Several examples of temporal imaging are given here to demonstrate the potential of our temporal zone plates to implement temporal imaging. However, the numerical simulations were not optimized. In practice, parameters such as temporal pulse width, repetition rate, dispersion amount, and time scale should be carefully optimized considering the experimental limitations.

#189054 - $15.00 USD Received 1 May 2013; revised 27 Jun 2013; accepted 28 Jun 2013; published 5 Jul 2013

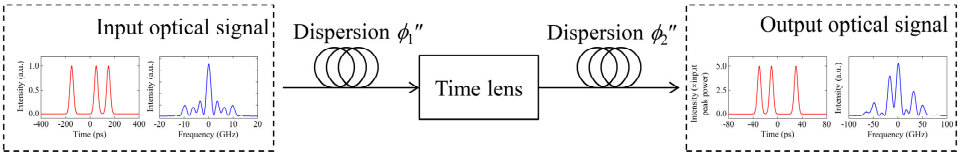

Fig. 15. Temporal imaging system, where the optical carrier frequency of input optical signal is 1550 nm, dispersion ϕ_1'' and ϕ_2'' are 10000 ps/nm and 2000 ps/nm, respectively.

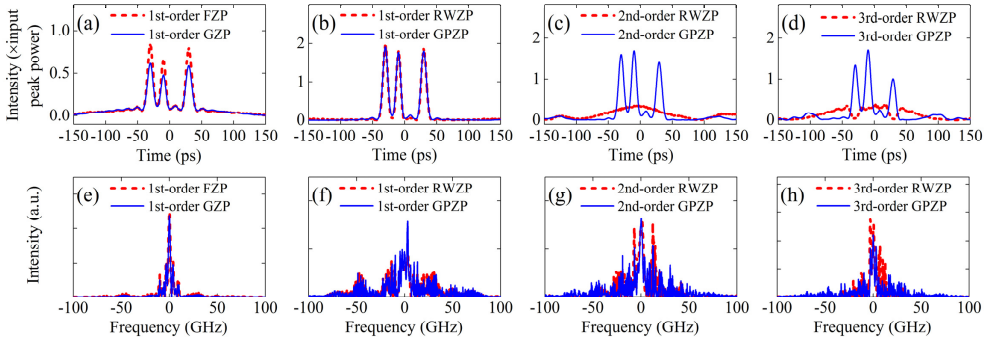

Fig. 16. The temporal intensity profiles (a)-(d) and spectra (e)-(h) of the output optical signals when the time lens in Fig. 15 is replaced with different zone plates.

5. Conclusions

In summary, two different kinds of temporal zone plates have been introduced and investigated, respectively based on temporal intensity modulation and temporal phase modulation. Temporal zone plates overcome the severe limitations on TBP (ratio between temporal aperture and resolution) of linear electro-optic time lenses. In particular, temporal zone plates can be ideally designed to offer a temporal aperture as large as desired, practically limited only by the amount of dispersion needed in the processing systems. Their time resolution depends inversely on the achievable temporal modulation bandwidth and operation order. In practice, only temporal phase zone plates, particularly GPZPs, of higher order ($|n|>1$) can be realistically implemented on the basis of their light-collecting efficiency performance. Hence, several times higher temporal resolutions can be achieved by use of high-order GPZPs. Additionally, the light-collecting efficiency in GPZPs can be optimized into the desired order by properly fixing the phase-modulation amplitude. Moreover, temporal phase zone plates offer higher light-collecting efficiency, leading to notably improved performance in pulse compression and temporal imaging systems, than their intensity-modulation counterparts.

The linear pulse compression experiments demonstrated here indicate that the temporal phase zone plate concept is a very promising approach to increase the energetic efficiency of previous schemes based on electro-optic time lenses by acting over longer input signal durations (higher input signal energies), leading to significantly increased output pulse peak powers. In the experiments reported here, we have obtained light-collecting efficiencies of 23.5%, 14.8%, and 9.4%, for temporal GPZPs of orders n = 1, 2, 3 respectively. Similar improvements may be anticipated for many other systems based on the use of time lenses by exploiting the significant TBP improvement offered by the temporal zone plate concepts introduced in this paper.

#189054 - $15.00 USD Received 1 May 2013; revised 27 Jun 2013; accepted 28 Jun 2013; published 5 Jul 2013

Acknowledgments

The authors thank the referees of the original submission of this paper for their meaningful and very useful feedback on the reported work, which has greatly helped to improve the overall quality of the final manuscript. The authors also express their gratitude to TeraXion Inc. for the loan of the LCFBG used in this work.

#189054 - $15.00 USD Received 1 May 2013; revised 27 Jun 2013; accepted 28 Jun 2013; published 5 Jul 2013